New BIOTECHNOLOGY 94 (2026) 253–263

Contents lists available at ScienceDirect

New BIOTECHNOLOGY

journal homepage: www.elsevier.com/locate/nbt

Advancements in cofactor regeneration for efficient UDP-GlcNAc and UDP-GalNAc synthesis

Benjamin Schmitz [a], Shubhang Sharma [b], Daniel Ohde [b,*], Andreas Liese [b], Lothar Elling [a,*]

[a] Laboratory for Biomaterials, Institute for Biotechnology and Helmholtz-Institute for Biomedical Engineering, RWTH Aachen University, Pauwelsstraße 20, Aachen 52074, Germany
[b] Institute of Technical Biocatalysis, Hamburg University of Technology, Denickestraße 15, Hamburg 21073, Germany

ARTICLE INFO

Keywords:
Nucleotide sugars
Multi-enzyme cascade
Cofactor regeneration
UDP-GlcNAc synthesis
UDP-GalNAc synthesis

ABSTRACT

UDP-GlcNAc and UDP-GalNAc are well-demanded nucleotide sugars and serve as precursors for the enzymatic synthesis of N- and O-glycans as well as glycosaminoglycans. Although the enzymatic synthesis cascade has been extensively studied, limitations remain for an efficient large-scale production. Unfavorable inhibitions by intermediate accumulation, precipitation of the byproduct phosphate with the needed cofactor magnesium, and efficient enzyme dosage still pose significant challenges. These challenges were investigated in an enzyme cascade including *N*-acetyl-hexosamine kinase from *Bifidobacterium longum* (*Bl*NahK), UDP-*N*-acetylgalactosamine diphosphorylase from *Homo sapiens* (*Hs*AGX1), and inorganic pyrophosphatase from *Pasteurella multocida* (*Pm*PpA) for UDP-GlcNAc and UDP-GalNAc synthesis. ATP supply started from AMP and polyphosphate by polyphosphate kinase from *Cytophaga hutchinsonii* (*Ch*PPK), and UTP was generated from UMP using cytidine/uridine monophosphate kinase from *Escherichia coli* (*Ec*CMPK) and cytidine/uridine diphosphate kinase from *Saccharomyces cerevisiae* (*Sc*CDPK). To reach a high productivity, enzyme cascade parameters were determined and optimized using Multiplex capillary electrophoresis. By kinetic modelling of the enzyme cascade and fine-tuning of the uncoupled UTP/ATP generation/regeneration system as well as observing the magnesium polyphosphate interplay with enzyme activity we were able to scale the production up to a molarity of 100 mM in 200 mL, yielding 10 g of UDP-GlcNAc with a conversion of 82.4% in 48 h and 12 g of UDP-GalNAc with full conversion in 29 h. The key limitations for successful scale-up, namely the promiscuity of *Bl*NahK towards UTP and interplay of magnesium ions with phosphate species, were overcome. Overall, the presented insights are expected to be transferable to similar enzyme cascades.

1. Introduction

Nucleotide sugars are well-demanded precursors as building blocks of different glycoconjugates, glycans, and polysaccharides. UDP-GlcNAc is no exception as part of glycosaminoglycans like hyaluronic acid with applications from cosmetics to biomedicine [1,2]. Enzymatically produced UDP-GlcNAc as a glycosylation precursor holds several advantages over common industrial processes like extraction or fermentation. The enzymatic route provides lower contamination risk of downstream glycosylated products. For instance, for hyaluronic acid, it also allows the possibility of controlling the final chain length of the glycopolymer [3]. Different production strategies have already been applied for UDP-GlcNAc, relying on a one-pot batch reaction either as is or in a repetitive batch mode, retaining enzymes after reaction by filtration and reusing them for another consecutive batch, making the process more enzyme load efficient [4–6]. UDP-GalNAc is a precursor to mucin-type O-glycans, partaking in cell signaling, immune defense, and lubrication, for instance, chondroitin sulfate, dermatan sulfate, heparin cofactor II, or hepatocyte growth factor [7]. UDP-GalNAc, a high-value nucleotide sugar, has been produced as well in batch or repetitive batch processes and a novel continuous fed-batch mode [5,6,8–10]. The main enzymes for the synthesis of UDP-GlcNAc and UDP-GalNAc make use of a salvage pathway consisting of NahK (*N*-acetyl-hexosamine kinase), either GlmU (*N*-acetylglucosamine−1- phosphate uridyltransferase) or AGX1 (UDP-*N*-acetylgalactosamine diphosphorylase), and PpA (inorganic pyrophosphatase) [8]. For nucleotide sugar production, ATP regeneration was deemed beneficial as high ADP concentrations can hinder diphosphorylase and kinase activity, and high ATP

* Corresponding authors.
E-mail addresses: daniel.ohde@tuhh.de (D. Ohde), l.elling@biotec.rwth-aachen.de (L. Elling).

https://doi.org/10.1016/j.nbt.2026.06.008
Received 21 January 2026; Received in revised form 24 June 2026; Accepted 25 June 2026
Available online 26 June 2026

concentrations can hinder kinase activity [10–15]. UTP cofactor generation was also considered as a cost factor in production and generated from uridine by ATP-dependent kinases and a polyphosphate kinase from *Ruegeria pomeroyi* (*Rp*PPK3, class I PPK2 phosphorylating nucleotide diphosphates [16]) using polyphosphate [10,14,15]. High regeneration cycles up to 240 without productivity loss compared to the original cascade were reported [15]. Magnesium phosphate and polyphosphate precipitation were reported to inactivate enzymes and limit intermediate concentration, resulting in low final product titer [9]. These limitations were tackled in a UDP-GalNAc and UDP-Gal synthesis utilizing kinetic modelling and DoE methodologies, but still the solubility of magnesium phosphate species remained a challenge [10,15]. Therefore, we decided to observe solubility separately as a prerequisite to ensuring cascade activity, as a classic multi-factor design of experiment approach might not capture solubility interactions to their full extent. In this study, we exploit kinetic relations in the cascade dictated by enzyme affinities, especially observing the magnesium polyphosphate and phosphate interplay and its effect on product yield and enzyme activity, to achieve high product titers (50–60 g/L). We also observed a competition between ATP and UTP as phosphate donors to *Bl*NahK, which led us to establish a novel enzyme cascade (Fig. 1) by uncoupling ATP regeneration and UTP generation. We selected the class III PPK2 (polyphosphate kinase from *Cytophaga hutchinsonii*), which phosphorylates nucleotide mono- and di phosphates [17], for ATP regeneration. We used a series reaction for generating UTP by selecting a combination of CMPK (cytidine/uridine monophosphate kinase) and CDPK (cytidine/uridine diphosphate kinase), which both utilize ATP for their respective phosphorylation. Contrary to earlier studies using polyphosphate kinases (**SI,** Figure S1), *Ch*PPK does not accept uridine phosphates [17,18], allowing for fine-tuning of ATP and UTP availability by changing PPK and kinase amounts rather than relying on the different affinities of PPK for adenosine and uridine phosphates [10,14,15]. The enzyme cascade was optimized for the production of multi-gram amounts of UDP-GlcNAc and UDP-GalNAc in a single one-pot batch reaction. Enzymes were used as lyophilizates to improve handling and storage, as well as uncoupling enzyme preparation from nucleotide sugar production, thereby further facilitating the process.

2. Materials and methods

2.1. Cascade enzymes

Backbone to all enzymes used in this study was the pET21b vector, including a C-terminal His_6-Tag to facilitate IMAC purification. *Bl*NahK, *Hs*AGX1, *Ec*CMPK, *Sc*CDPK, and *Pm*PpA vectors were already available as described in earlier studies [3–5,9,13]. The utilized PPK was derived from *Cytophaga hutchinsonii* (ATCC 33406), and the plasmid was synthesized by BioCat (Heidelberg, Germany) (**SI,** Figure S2). Each enzyme was codon optimized for recombinant expression in *E. coli* and contained a selection marker for ampicillin.

2.2. Protein expression and purification

For every enzyme, a colony of transformed *E. coli* BL21 (DE3) cells

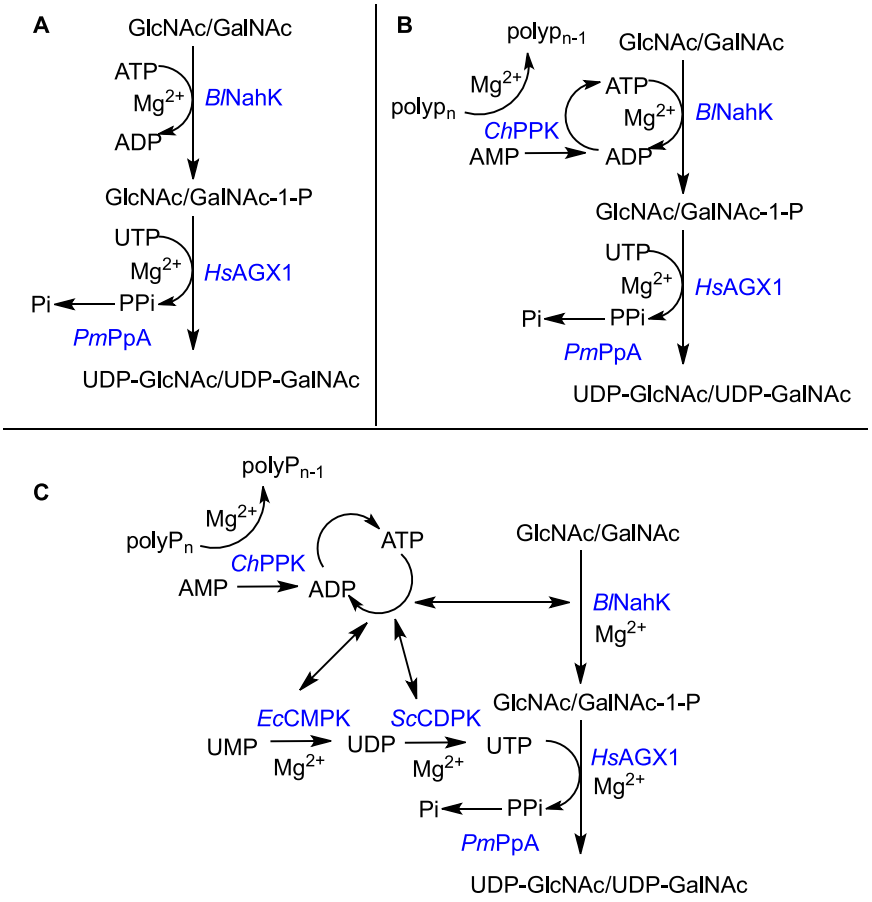

Fig. 1. Multi-enzyme cascade for the production of UDP-GlcNAc and UDP-GalNAc. Cascade A: Basic cascade for UDP-GlcNAc and UDP-GalNAc synthesis. Cascade B: UDP-GlcNAc and UDP-GalNAc cascade with ATP generation/regeneration. Cascade C: UDP-GlcNAc and UDP-GalNAc cascade with ATP generation/regeneration and UTP generation. *Bl*NahK: NahK (*N*-acetyl hexosamine kinase from *Bifidobacterium longum*, *Hs*AGX1; UDP-*N*-acetylgalactosamine diphosphorylase from *Homo sapiens*, *Ch*PPK: polyphosphate kinase from *Cytophaga hutchinsonii*, *Ec*CMPK: cytidine/uridine diphosphate kinase from *Escherichia coli*, *Sc*CDPK: cytidine/uridine diphosphate kinase from *Saccharomyces cerevisiae*, *Pm*PA: inorganic pyrophosphatase from *Pasteurella multocida*.

was picked and grown overnight at 37 °C in 5 mL LB-medium containing 100 μg*mL^{-1} ampicillin at 120 rpm as a pre-culture. The main expression was carried out in 1 L TB-medium inoculated with the full preculture. Expression was induced after growth to an approximate OD of 0.6 at 37 °C and 80 rpm with 0.1 mM IPTG. After induction temperature was kept at 25 °C for 16–20 h. Cells were harvested by centrifugation at 7000 rpm at 4 °C for 30 min and prepared for purification by resuspension of 4 g in 10 mL IMAC binding buffer (20 mM HEPES-NaOH, 500 mM NaCl, 30 mM imidazole, pH 7.4) and sonication for 6.5 min with 15 s pulses followed by 60 s pauses at 52% amplitude. Enzymes were purified by IMAC, carried out on an Äkta system equilibrated and washed with IMAC binding buffer, and eluted with IMAC elution buffer (20 mM HEPES-NaOH, 500 mM NaCl, 500 mM imidazole, pH 7.4). Enzyme-containing fractions were pooled, rebuffered in 100 mM HEPES-NaOH, pH 8, by dialysis, and lyophilized at −60 °C and < 0.1 mbar overnight. Lyophilizates were stored at −80 °C, lyophilized enzymes were resuspended as needed, and their concentration was determined using a standard Bradford assay.

2.3. MP-CE analysis

Quantification of sugar nucleotides and nucleotides was performed by multiplex capillary electrophoresis (MP-CE, cePro 9600™ system by Advanced Analytical Technologies) using an ammonium acetate buffer (70 mM NH_4Ac, 1 mM EDTA, pH 9.2) and a separation voltage of 10 mM [19]. Capillaries had an effective length of 55 cm, a total length of 80 cm, and an inner diameter of 50 μM. Eluted peaks were quantified by UV absorbance at 254 nm. Samples were prepared in a 96-well PCR plate with a volume of 30 μL and injected by vacuum at −0.7 psi. Internal standards were para-aminophthalaic acid (PAPA) and para-aminobenzoic acid (PABA). Analyte molecules were quantified with standards (**SI,** Figure S3 **-** Figure S9).

2.4. Activity assays

Enzyme activity was determined before and after lyophilization. Assays were conducted in 300 μL at 37 °C; common components for all assays were 50 mM $MgCl_2$ and 200 mM HEPES-NaOH at pH 8. Each enzyme activity was determined with substrate saturation at 10 mM ATP and GlcNAc for *Bl*NahK, 10 mM UTP and GlcNAc−1-phosphate for *Hs*AGX1, 10 mM ADP/AMP and 70 mM polyphosphate (average chain length 25) for *Ch*PPK, 10 mM UMP and ATP for *Ec*CMPK, and 10 mM UDP and ATP for *Sc*CDPK. Reactant concentrations were determined by MP-CE. The specific enzyme activity was calculated (Eq. 1).

$$A_{specific} = \frac{k * df}{c_m} \tag{1}$$

The slope of the product formation is k in μMol*min^{-1}, the dilution factor of the enzyme is df, and the mass concentration of the enzyme is c_m.

2.5. Kinetic measurements

Enzyme kinetics were determined for *Ch*PPK, *Ec*CMPK, and *Sc*CDPK as *Bl*NahK, and *Hs*AGX1 kinetics have already been determined in previous works [20,21]. All enzymes rely on at least two substrates, so kinetics were measured accordingly while keeping one substrate at saturation and varying the other. Inhibition constants were evaluated at key points with substrate concentrations near v_{max} and K_M. For *Ch*PPK, AMP/ADP was kept constant at 10 mM and varied between 250 μM and 7.5 mM. Polyphosphate was kept constant at 100 mM and varied between 2.5 mM and 100 mM. phosphate/pyrophosphate inhibition was determined at 100 mM polyphosphate and 10 mM ADP, as well as 8 mM polyphosphate and 10 mM ADP, with phosphate/pyrophosphate varying from 2.5 mM to 100 mM. The influence of $MgCl_2$ on reaction velocity was observed between 2.5 mM and 100 mM. *Ec*CMPK and *Sc*CDPK kinetics were obtained for ATP and UMP or UDP, respectively, with the constant substrate at 10 mM and the varying substrate at 0.5 mM to 10 mM. Generally, HEPES-NaOH buffer was at 200 mM with pH 8, temperature at 37 °C, and $MgCl_2$ at 50 mM if not varied for kinetics regarding $MgCl_2$. Reactant concentrations were determined by MP-CE. Reaction velocities were computed as described for activity assays (Eq. 1).

2.6. Kinetic modelling

The collected kinetic data were fitted to appropriate models for the two-substrate enzymes, a random or ordered sequential mechanism, which are represented by the same model, and for single-substrate enzymes, the standard Michaelis-Menten model. The measured data points for reaction rate as a function of substrate concentration were evaluated against the model with the negative log predictive density and minimized for the model fit (Eq. 2).

$$NLPD = -\sum_{i=1}^{N} \log p(y_i = t_i | x_i) \tag{2}$$

The errors in the parameter estimation for the kinetic parameters were determined using the NLPD Fisher information matrix at the point of parameter estimation (Eq. 3).

$$I(\theta) = \frac{\partial^2}{\partial\theta_i * \partial\theta_j} * NLPD(\theta) \tag{3}$$

The square root of the diagonal elements of the covariance matrix, which corresponds to the negative inverse of the Fisher information matrix, provides the errors in the parameter estimation (Eq. 4).

$$SE = \sqrt{diag\left(-I(\theta)^{-1}\right)} \tag{4}$$

Inhibition constants were determined from a linear fit of the inverse reaction velocity as a function of inhibitor concentration. K_I corresponds to the intercept divided by the slope of the linear fit. The errors in v_{max} were scaled according to the inverse transformation. The error in the parameter estimate was calculated directly from the square root of the diagonal elements of the covariance matrix.

Non-experimentally determined inhibition constants were computed by least square fitting deviations of experimental compared to simulated cascade molecule progressions.

The Python packages scipy, jax, and numpy were used for fitting [22–24].

2.7. Cascade optimization

The model of the overall cascade is described by a system of ordinary differential equations for the rates of change of the molecules involved. These rates in turn depend on the reaction rates of the enzymes, which depend on their substrate and inhibitor concentrations (Eqs. 5–16). Rate equations for *Bl*NahK and *Hs*AGX1 are used for GalNAc with the respective reaction rates as well.

$$\frac{dpolyP}{dt} = -v_{PPK,1} - v_{PPK,2} \tag{5}$$

$$\frac{dAMP}{dt} = -v_{PPK,1} \tag{6}$$

$$\frac{dADP}{dt} = v_{PPK,1} + v_{CMPK} + v_{CDPK} + v_{NahK,1} - v_{PPK,2} \tag{7}$$

$$\frac{dATP}{dt} = v_{PPK,2} - v_{CMPK} - v_{CDPK} - v_{NahK,1} \tag{8}$$

$$\frac{dUMP}{dt} = -v_{CMPK} \quad (9)$$

$$\frac{dUDP}{dt} = v_{CMPK} + v_{NahK,2} - v_{CDPK} \quad (10)$$

$$\frac{dUTP}{dt} = v_{CDPK} - v_{NahK,2} - v_{AGX1} \quad (11)$$

$$\frac{dGlcNAc}{dt} = -v_{NahK,1} - v_{NahK,2} \quad (12)$$

$$\frac{d\mathrm{GlcNAc-1-P}}{dt} = v_{NahK,1} + v_{NahK,2} - v_{AGX1} \quad (13)$$

$$\frac{d\mathrm{UDP-GlcNAc}}{dt} = v_{AGX1} \quad (14)$$

$$\frac{dPPi}{dt} = v_{AGX1} - v_{PpA} \quad (15)$$

$$\frac{dPi}{dt} = 2 * v_{PpA} \quad (16)$$

This system of equations can be solved by numerical integration to obtain a concentration curve of the molecules over time for fixed initial conditions of initial molecule concentrations and enzyme quantities. Suitable initial conditions for the system can now be found with the help of an optimization target in order to meet this target in the best possible way. The aim of the optimization was an efficient use of enzymes and the lowest possible accumulation of molecules in the intermediate steps under the condition that a hard constraint for an almost complete conversion at a fixed point in time should be met (Eq. 17). For equal weighting, values were normalized in reference to sums at upper optimization bounds.

$$f_{\min} = \frac{1}{w_{R,1}} * \sum_{i=1}^{N} m_{E,i} + \frac{1}{w_{R,2}} * \sum_{j=1}^{M} \int_{t_0}^{t_{end}} [S_j] \quad (17)$$

2.8. UDP-GlcNAc synthesis

UDP-GlcNAc synthesis was done with three different cascade compositions. The basic cascade consisted of *Bl*NahK, *Hs*AGX1, and *Pm*PpA for sugar phosphorylation, synthesizing UDP-GlcNAc from UTP and GlcNAc-1-P, and cleaving the pyrophosphate byproduct, respectively (Fig. 1**A**). ATP regeneration/generation with polyphosphate was achieved by the addition of *Ch*PPK (Fig. 1**B**). The final system additionally included UTP regeneration/generation by *Ec*CMPK and *Sc*CDPK (Fig. 1**C**). All syntheses were carried out at 37 °C and pH 8, buffered by HEPES-NaOH. Small-scale syntheses were carried out in a 300 µL volume; larger-scale ones were first scaled to 1 mL, then to 20 mL, and then to 200 mL. Targeted concentrations for the conversion of GlcNAc to UDP-GlcNAc were 10 mM, 50 mM, and 100 mM. Reactions to establish the regeneration cassette were run in 300 µL with 10 mM GlcNAc. The target concentration for UDP-GalNAc synthesis was 100 mM.

2.8.1. Enzyme cascade A

Cascade A (300 µL) was carried out with *Bl*NahK (0.16 mg, 0.2 U), *Hs*AGX1 (0.18 mg, 1 U), *Pm*PpA (0.2 mg), 10 mM GlcNAc, 10 mM ATP, 10 mM UTP, and 50 mM $MgCl_2$.

2.8.2. Enzyme cascade B

Cascade B (300 µL) with ATP generation/regeneration contained *Ch*PPK (0.133 mg, 2 U), *Bl*NahK (0.31 mg, 0.4 U), *Hs*AGX1 (0.035 mg, 0.2 U), *Pm*PpA (0.2 mg), 10 mM GlcNAc, 20 µM AMP, 10 mM polyphosphate, 10 mM UTP, and 50 mM $MgCl_2$.

2.8.3. Enzyme cascade C

Cascade C (300 µL) with UTP generation/regeneration contained *Ch*PPK (0.663 mg, 10 U), *Ec*CMPK (0.145 mg, 0.4 U), *Sc*CDPK (0.0078 mg, 0.8 U), *Bl*NahK (0.16 mg, 0.2 U), *Hs*AGX1 (0.07 mg, 0.4 U), *Pm*PpA (0.2 mg), 70 mM polyphosphate, 50 mM $MgCl_2$, 25 mM UMP, 10 mM GlcNAc, and 3 mM AMP. The synthesis to assess the developed cascade model was carried out in the same scope with *Ch*PPK (0.663 mg, 10 U), *Ec*CMPK (0.145 mg, 0.4 U), *Sc*CDPK (0.0078 mg, 0.8 U), *Bl*NahK (0.16 mg, 0.2 U), *Hs*AGX1 (0.07 mg, 0.4 U), *Pm*PpA (0.2 mg), 70 mM polyphosphate, 10 mM UMP, 10 mM GlcNAc, and 2.5 mM AMP.

Magnesium polyphosphate screening was performed in 300 µL and 50 mM substrate with *Ch*PPK (0.2 mg, 3.01 U), *Ec*CMPK (0.1 mg, 0.28 U), *Sc*CDPK (0.1 mg, 10.36 U), *Bl*NahK (0.2 mg, 0.26 U), *Hs*AGX1 (0.2 mg, 1.16 U), *Pm*PpA (0.2 mg), 50–200 mM polyphosphate, 10–350 mM $MgCl_2$, 2 mM AMP, 50 mM UMP, and 50 mM GlcNAc.

This reaction was scaled to 1 mL with *Ch*PPK (0.66 mg, 9.95 U), *Ec*CMPK (0.33 mg, 0.92 U), *Sc*CDPK (0.33 mg, 34.18 U), *Bl*NahK (0.66 mg, 0.86 U), *Hs*AGX1 (0.66 mg, 3.83 U), *Pm*PpA: (0.66 mg), 50–250 mM polyphosphate, 20–100 mM $MgCl_2$, 2 mM AMP, 50 mM UMP, and 50 mM GlcNAc.

A synthesis in 1 mL volume was carried out at 100 mM substrate with *Ch*PPK (1.32 mg, 19.91 U), *Ec*CMPK (0.66 mg, 1.83 U), *Sc*CDPK (0.66 mg, 68.37 U), *Bl*NahK (1.32 mg, 1.72 U), *Hs*AGX1 (1.32 mg, 7.66 U), *Pm*PpA (1.32 mg), 500 mM polyphosphate, 200 mM $MgCl_2$, 4 mM AMP, 100 mM UMP, and 100 mM GlcNAc.

The reaction with high molarity of substrates was further scaled to 20 mL with *Ch*PPK (13.2 mg, 199.06 U), *Ec*CMPK (6.6 mg, 18.28 U), *Sc*CDPK (6.6 mg, 683.70 U), *Bl*NahK (13.2 mg, 17.16 U), *Hs*AGX1 (13.2 mg, 76.56 U), and *Pm*PpA (13.2 mg). The reaction in a 200 mL scale contained *Ch*PPK (100 mg, 1508.00 U), *Ec*CMPK (60 mg, 166.20 U), *Sc*CDPK (40 mg, 4143.60 U), *Bl*NahK (150 mg, 195.00 U), *Hs*AGX1 (140 mg, 812.00 U), and *Pm*PpA (70 mg).

Enzymes from the 20 mL reaction were recovered between batches by centrifugation in a VivaSpin column (10 kD MWCO) at 5000 rpm. The 200 mL batch was shaken at 100 rpm. All samples taken were stopped with 50% (v/v) stop solution (14 mM SDS, 2 mM PAPA, 2 mM PABA) and, if necessary, diluted to an appropriate concentration beforehand.

2.9. UDP-GlcNAc and UDP-GalNAc isolation

UDP-GlcNAc and UDP-GalNAc were precipitated by isopropanol with an already described methodology [11]. First, remaining nucleotides were digested with alkaline phosphatase (SEVA, Heidelberg) and precipitated with 40% (v/v) isopropanol after 30 min incubation at −20 °C. The precipitate was pelleted by centrifugation and discarded. The supernatant was then again incubated for 30 min with 80% (v/v) isopropanol at −20 °C, and the heavier phase was collected with a separating funnel for lyophilization. The lyophilizate was analyzed by capillary electrophoresis and HPLC ESI-MS.

2.10. HPLC ESI-MS

Synthesized UDP-GlcNAc and UDP-GalNAc were checked by reversed-phase high-performance liquid chromatography (HPLC) coupled to an electrospray ionization mass spectrometer (ESI-MS). Analytes were separated by an isocratic eluent (15% (v/v) acetonitrile, 85% (v/v) water) on a Multospher 120 RP 18 HP−3µ column. For ESI-MS needle voltage was 4 kV, the temperature was 400 °C, the cone voltage was 100 V, and negative mode was used. Analyte masses were determined by their mass/charge-ratio (*m/z*).

3. Results

3.1. Cascade enzymes

All cascade enzymes were obtained with yields between 7 and 40 mg enzyme per gram cell wet weight (CWW) with *Pm*PpA at the highest and *Ec*CMPK at the lowest. The lyophilized enzymes retained 78–95% of their specific activity (**SI,** Table S1). Their storage stability was determined at a half-life of 20 weeks (**SI,** Figure S10). Additionally, previously described difficulty in expressing *Ch*PPK due to inclusion bodies [17] was overcome by using a fusion construct with maltose-binding protein (MBP) as a solubility tag, which renders PPK as one of the enzymes with the highest expression yield in this study. The MBP-tag was not cleaved from the fusion construct to further facilitate solubility in the batch application of *Ch*PPK.

3.2. Nucleotide regeneration cassettes

Already known inhibitions of the reaction cascade by high nucleotide concentrations either reduce product formation or increase the amount of enzyme required for compensation many times over [13]. In enzyme cascade A (Fig. 1**A**), an initial lag phase and later deviation between ADP (10 mM) and UDP-GlcNAc (8.5 mM) concentration were observed, which is caused by inhibition of *Bl*NahK at high ATP concentrations and of *Hs*AGX1 at high ADP concentrations [12] (Fig. 1**A**). As addressed in established syntheses, regeneration of ATP *in situ* offers a solution [10, 13,14]. ATP generation/regeneration from 20 μM AMP (Fig. 1**B**), based on polyphosphate by *Ch*PPK, was able to overcome the initial lag phase (Fig. 2**B**).

However, enzyme cascade B showed a reduction in product yield of 61% (6.1 mM), and the formation of UDP was observed during the synthesis. We concluded that *Bl*NahK used UTP as a competitor to ATP, particularly at a low ATP concentration of 20 μM (Fig. 2**B**). This substitution highlights the promiscuous nature of *Bl*NahK, resulting in byproduct UDP formation, which remains unavailable for the pyrophosphorylase reaction by *Hs*AGX1. Stoichiometric evaluation gave conclusive evidence that 3.5 mM GlcNAc was phosphorylated by utilizing UTP, forming 3.5 mM UDP-GlcNAc and 3.5 mM UDP as byproducts. Hence, in the generation of the remaining 2.6 mM UDP-GlcNAc, ATP was regenerated 130 times by *Ch*PPK during GlcNAc phosphorylation.

To address the bias of *Bl*NahK for ATP and UTP, the regeneration cassette was expanded to include *Ec*CMPK and *Sc*CDPK, which convert UMP to UTP, supplying it steadily at lower concentrations, thus mitigating the competition for ATP (Fig. 1**C**). In addition to compensating for the remaining UTP consumption by *Bl*NahK by regeneration, this allows the use of the significantly cheaper UMP, which represents one of the major cost factors in the synthesis. Including the regeneration of ATP by *Ch*PPK for three kinases in the cascade, polyphosphate concentration is a crucial factor to supply UTP for product formation. If the polyphosphate threshold in the reaction was too low, the reversed reaction of *Ec*CMPK supplied *Bl*NahK with ATP instead of PPK (**SI,** Figure S11). Therefore, we assessed product formation and uridine phosphate availability depending on polyphosphate concentration (Fig. 3)

UDP-GlcNAc formation is directly linked to the amount of supplied polyphosphate, as ATP has to be regenerated three times per one UDP-GlcNAc formed. With 30–50 mM polyphosphate, 3–5 mM UDP-GlcNAc is synthesized. With 60 mM to 80 mM polyphosphate, 7.5 mM UDP-GlcNAc are obtained. Additionally, polyphosphate concentration, being a contributor to PPK reaction velocity, dictates overall product formation rate through the concentration of supplied ATP. In this reaction setup, 60–80 mM of polyphosphate promoted efficient UDP-GlcNAc and UTP formation. Restrictions in product formation for polyphosphate concentrations of 30–50 mM occurred most likely due to competition of *Ec*CMPK, *Sc*CDPK, and *Bl*NahK for the small 20 μM ATP pool provided by *Ch*PPK. 70 mM of polyphosphate was chosen for the next batch synthesis, as the phosphorylation threshold thereof was deemed sufficient. With a larger AMP pool of 3 mM and UMP excess, UTP and GlcNAc-1-phosphate availability could be provided to a greater extent, and full conversion of GlcNAc to UDP-GlcNAc was achieved (**SI,** Figure S12). Still, due to UMP excess, the amount of remaining nucleotides was high.

3.3. Kinetic modelling of the enzyme cascade

To increase the efficiency of the synthesis, in particular by reducing the amount of enzyme used to a minimum and preventing the accumulation of intermediates, kinetic data were collected for all enzymes involved (Table 1**,** **SI,** Figure S13-S27).

As the ATP pool in the cascade has to be shared between all ATP-dependent kinases, their affinity towards ATP is decisive for determining which concentration is needed to operate at full efficiency. *Ec*CMPK ($K_{M,\ ATP}$ 0.1 mM) showed the highest affinity, followed closely by *Bl*NahK ($K_{M,\ ATP}$ 0.1 mM), whereas *Sc*CDPK ($K_{M,\ ATP}$ 0.83 mM) had the lowest affinity. However, the maximum reaction velocity of *Bl*NahK and *Ec*CMPK is dictated by their affinity towards GlcNAc ($K_{M,\ GlcNAc}$ 1.8 mM) and UMP ($K_{M,\ UMP}$ 4.05 mM), respectively, while *Sc*CDPK shows a lower affinity for its second substrate ($K_{M,\ UDP}$ 0.29 mM). Therefore, UTP and ATP availability must be balanced, because *Bl*NahK ($K_{M,\ UTP}$ 2.0 mM) and *Hs*AGX1 ($K_{M,\ UTP}$ 0.053 mM) will compete for UTP at high UTP concentrations and low ATP concentrations (Fig. 2**B**). Thus, on one hand, reaction velocity for UTP provision has to be closely tied to

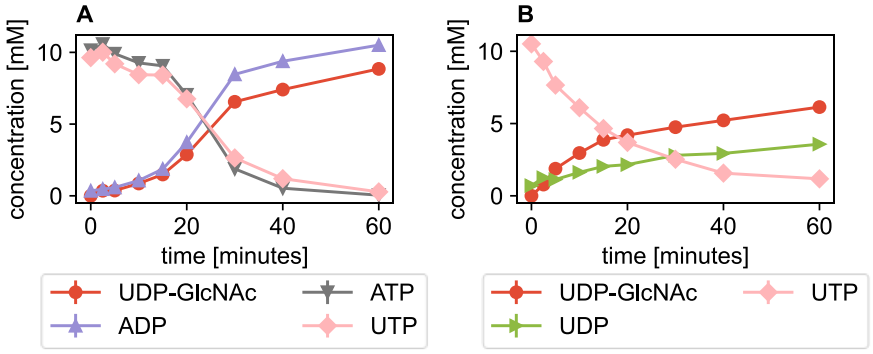

Fig. 2. A Batch synthesis of UDP-GlcNAc (cascade A). Reaction conditions: *Bl*NahK: 0.16 mg (0.2 U), *Hs*AGX1: 0.18 mg (1 U), *Pm*PpA: 0.2 mg, 10 mM GlcNAc, 10 mM ATP, 10 mM UTP, 50 mM $MgCl_2$, 100 mM carbonate buffer pH 8 in 300 μL, 37 °C. **B Batch synthesis of UDP-GlcNAc with ATP generation/regeneration system (cascade B).** Reaction conditions: *Ch*PPK: 0.133 mg (2 U), *Bl*NahK: 0.31 mg (0.4 U), *Hs*AGX1: 0.035 mg (0.2 U), *Pm*PpA: 0.2 mg, 10 mM GlcNAc, 20 μM AMP, 10 mM polyphosphate, 10 mM UTP, 50 mM $MgCl_2$, 100 mM carbonate buffer pH 8 in 300 μL, 37 °C. Samples were measured in technical triplicates and standard deviations are shown as error bars (SI, Table S2-S3).

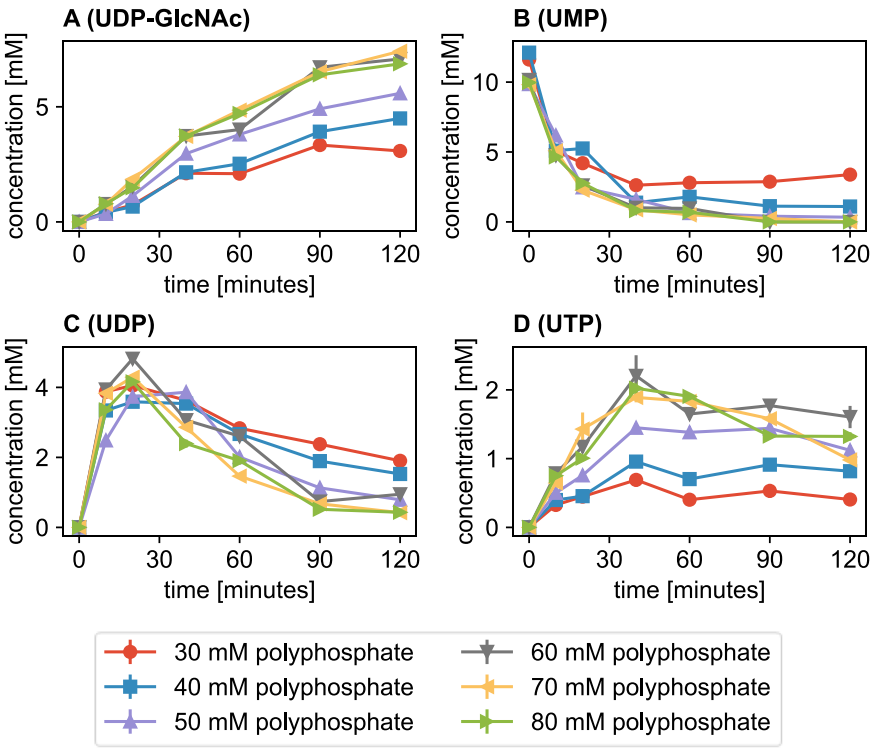

Fig. 3. UDP-GlcNAc formation and uridine nucleotide availability at varying polyphosphate concentrations. Reaction conditions: *Ch*PPK: 0.663 mg (10 U), *Ec*CMPK: 0.145 mg (0.4 U), *Sc*CDPK: 0.0078 mg (0.8 U), *Bl*NahK: 0.31 mg (0.4 U), *Hs*AGX1: 0.035 mg (0.2 U), *Pm*PpA: 0.2 mg, 10 mM GlcNAc, 20 µM AMP, 30–80 mM polyphosphate, 10 mM UMP, 50 mM $MgCl_2$, 100 mM sodium bicarbonate buffer pH 8 in 300 µL, 37 °C. A UDP-GlcNAc, B UMP, C UDP, D UTP. Samples were measured in technical triplicates and standard deviations are shown as error bars (SI, Table S4-S9).

Table 1
Kinetic data of all cascade enzymes.

Enzyme	Substrate	Inhibitors	K_M [mM]	K_I [mM]	v_{max} [U *mg^{-1}]
*Ch*PPK	AMP	-	12.09	-	76.03
	ADP	-	0.75	-	15.05
	polyphosphate	-	9.12	-	-
	-	P_i	-	65.56	-
	-	PP_i	-	22.77	-
*Ec*CMPK	ATP	-	0.1[a]	-	3.89
	UMP	-	4.05	-	
		P_i[b]	-	2.93	
*Sc*CDPK	ATP	-	0.83	-	103.59
	UDP	-	0.29	-	
		P_i[b]	-	0.76	
*Bl*NahK	ATP*	-	0.1	-	1.3
	GlcNAc*	-	1.8	-	
	UTP	-	8.54	-	0.68
	GlcNAc	-	0.56	-	
	ATP	-	1.96	-	1.46
	GalNAc		5.01	-	
	UTP		101.03	-	6.66
	GalNAc		2.39	0.14	
		P_i[b]	-	4.38	
*Hs*AGX1	UTP*	-	0.053	-	5.8
	GlcNAc−1-P*	-	0.032	-	
	UTP*	-	0.053	-	14.9
	GalNAc−1-P*	-	0.38	-	
		P_i[b]	-	0.99	

* Kinetics of *Bl*NahK[21] and *Hs*AGX1[20] were derived from literature for similar reaction conditions

[a] Was below the MP-CE detection limit of 0.1 mM; for modelling purposes, it was assumed as 0.1 mM.

[b] Inhibitor constants for Pi of *Ec*CMPK, *Sc*CDPK, *Bl*NahK, and *Hs*AGX1 were determined by reverse fitting of the model to experimental data

UTP consumption velocity by *Hs*AGX1. On the other hand, fast maintenance of the ATP pool by regeneration *via* *Ch*PPK has to be ensured. Noticeably, contrary to earlier findings ($K_{M,\ AMP}$ 0.62 mM, $K_{M,\ ADP}$ 0.35 mM [17]), *Ch*PPK prefers phosphorylating ADP ($K_{M,\ ADP}$ 0.75 mM) over AMP ($K_{M,\ AMP}$ 12.09 mM), making the regeneration of ATP from ADP the predominant reaction over ATP generation starting with AMP. This shows that *Ch*PPK supplied with AMP yields both ADP and ATP right from reaction beginning on. Furthermore, the applied enzyme units in the cascade of ATP using kinases have to be balanced, because *Bl*NahK and *Ec*CMPK will compete for ATP. If ATP is scarcely available, either UTP or GlcNAc-1-P synthesis will be preferred depending on enzyme affinity and amount. This leaves *Hs*AGX1 missing one necessary substrate, delaying UDP-GlcNAc formation. $K_{I,\ Pi}$ for *Ec*CMPK, *Sc*CDPK, *Bl*NahK, and *Hs*AGX1 were determined by comparing experimental to simulated cascade progression data and least square fitting. All kinetic data were fitted to the appropriate models, and formulas for the reaction rates were determined (**SI,** Table S10). The reaction rates of the enzymes were used to simulate the change in molecule concentrations over the course of the synthesis. The initial conditions for solving the system were the same as those for which data points on the reaction process had already been recorded (Fig. 4).

The 10 mM synthesis is generally well described by the developed model, with sufficiently accurate concentration predictions. However, ATP formation by *Ch*PPPK is overestimated. This is most likely caused by the lack of consideration of reversible reactions and the inactivation of the enzymes over the reaction time in the model. In addition, the entire reaction system is dependent on the magnesium content in the solution, which changes over the course of the reaction due to the interaction with the various phosphate species, namely ortho phosphate, pyrophosphate, and polyphosphate. This has a significant influence on the function and reaction rate of the enzymes.

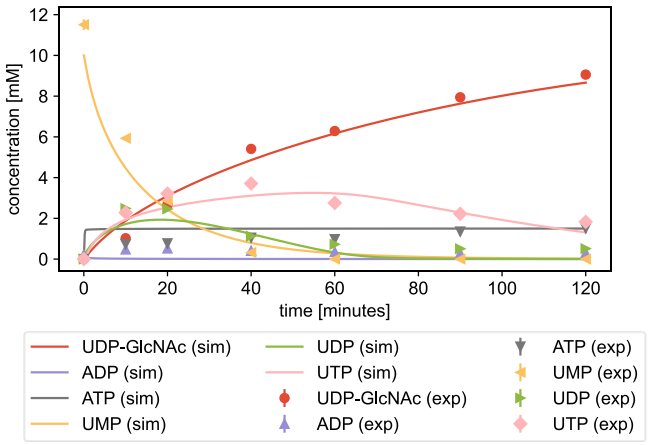

Fig. 4. Modelling of the batch synthesis of UDP-GlcNAc with ATP/UTP regeneration/generation and comparison to measured data. Model conditions: *Ch*PPK: 0.663 mg (10 U), *Ec*CMPK: 0.145 mg (0.4 U), *Sc*CDPK: 0.0078 mg (0.8 U), *Bl*NahK: 0.08 mg (0.1 U), *Hs*AGX1: 0.07 mg (0.4 U), *Pm*PpA: 0.2 mg, 70 mM polyphosphate, 10 mM UMP, 10 mM GlcNAc, 1.5 mM AMP. Reaction conditions: *Ch*PPK: 0.663 mg (10 U), *Ec*CMPK: 0.145 mg (0.4 U), *Sc*CDPK: 0.0078 mg (0.8 U), *Bl*NahK: 0.16 mg (0.2 U), *Hs*AGX1: 0.07 mg (0.4 U), *Pm*PpA: 0.2 mg, 70 mM polyphosphate, 50 mM $MgCl_2$, 10 mM UMP, 10 mM GlcNAc, 2.5 mM AMP, 200 mM HEPES-NaOH pH 8 in 300 µL, 37 °C. Samples were measured in technical triplicates and standard deviations are shown as error bars (SI, Table S11).

3.4. Magnesium phosphate

Scaling the optimized enzyme cascade for 10 mM to 50 mM GlcNAc, the interaction of magnesium and the phosphate species proved to be a particular challenge. Magnesium supply for all enzymes was limited by high polyphosphate concentrations and magnesium phosphate precipitation. In the enzyme cascade, phosphate concentration is tied to product formation. The deciding factor for cascade performance regarding magnesium phosphate solubility is both the initially supplied magnesium and polyphosphate concentration. Thus, product formation was evaluated for different combinations of magnesium polyphosphate for 50 mM GlcNAc after a 90-minute reaction time (Fig. 5, **SI,** Figure S28).

The lattice from 10 to 350 mM $MgCl_2$ and 50–200 mM polyphosphate showed a distinct region of the enzyme cascade system activity at polyphosphate concentrations that were 2.5 times higher than $MgCl_2$ concentrations. Besides this region, cascade activity was very low with observable precipitation and therefore not suited for further consideration for efficient synthesis. Four different polyphosphate-

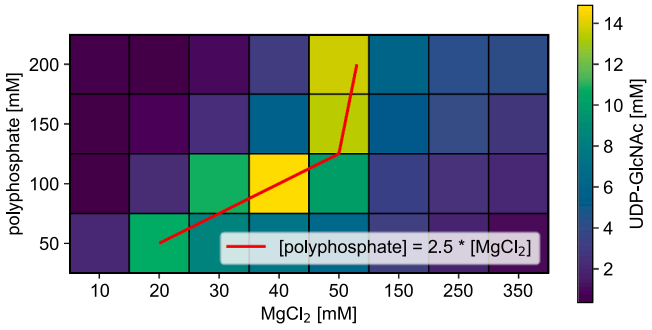

Fig. 5. UDP-GlcNAc formation dependency on different magnesium polyphosphate concentrations. Reaction conditions: *Ch*PPK: 0.2 mg (3.01 U), *Ec*CMPK: 0.1 mg (0.28 U), *Sc*CDPK: 0.1 mg (10.36 U), *Bl*NahK: 0.2 mg (0.26 U), *Hs*AGX1: 0.2 mg (1.16 U), *Pm*PpA: 0.2 mg, 50–200 mM polyphosphate, 10–350 mM $MgCl_2$, 2 mM AMP, 50 mM UMP, 50 mM GlcNAc, 200 mM HEPES-NaOH pH 8 in 300 µL, reaction time 90 min at 37 °C.

$MgCl_2$ combinations with a concentration ratio of 2.5 (50 mM - 20 mM, 100 mM - 40 mM, 125 mM - 50 mM, and 250 mM - 100 mM) were chosen for the conversion of 50 mM GlcNAc (Fig. 6).

The cascade system was, as expected, active with every polyphosphate-$MgCl_2$ combination. However, as observed beforehand (Fig. 3), the polyphosphate concentration influences the phosphorylation capacity of the cascade. There was a linear relationship between polyphosphate concentration and achievable conversion percentage. This, in turn, indicates as hypothesized before that just a small fraction of the general phosphorylation capability of polyphosphate is utilized by the PPK and that higher molarity syntheses have to be scaled accordingly.

3.5. UDP-GlcNAc synthesis

For UDP-GlcNAc production, 100 mM substrate conversion was targeted. To achieve this, optimal conditions for 50 mM conversion were scaled linearly (**SI,** Figure S29). With chosen cascade system parameters, 100 mM substrate could be fully converted to UDP-GlcNAc in the same time scope as for 50 mM substrate. While starting with a steep increase for 3 h up to 40 mM UDP-GlcNAc, product formation velocity slowed down after that point, where enzyme affinities and degradation are not expected to play a significant role yet. This phenomenon can be attributed to phosphate accumulation as a side product, which steadily deprives the enzymes of magnesium by precipitation. Still, product formation is well described by the model, even though the overall conversion was underestimated. As a next step, the 100 mM cascade system was further upscaled to a 20 mL reaction volume, and a repetitive batch approach was assessed (**SI,** Figure S30). Here as well, the cascade system upheld full conversion in the scope of 24 h, although enzyme concentrations were halved compared to the 1 mL batch. This indicates that enzyme reaction velocity is most likely closely tied to the available magnesium concentration in solution and thereby limited. However, cascade activity was very low for the second batch, making a repetitive approach not suitable for synthesis. With the first batch achieving full conversion, a further tenfold scale-up to 200 mL has been carried out (Fig. 7).

After 48 h, 82.4% conversion was reached, amounting to 10 g UDP-GlcNAc. The total turnover number (TTN), space-time yield (STY), and average productivity were 16.95 $g_P*g_E^{-1}$, 1.04 $g*L^{-1}h^{-1}$, and 0.21 $g*h^{-1}$, respectively. Product formation was well described by the model. UDP-GlcNAc was isolated by isopropanol precipitation at 24.6% purity with a 2.37 g (23.7%) yield. UDP-GlcNAc isolation was confirmed by HPLC ESI-MS (**SI,** Figure S31).

3.6. UDP-GalNAc synthesis

The same cascade can also synthesize UDP-GalNAc; however, different activities and affinities for GalNAc and GalNAc−1-phosphate for *Bl*NahK and *Hs*AGX1 have to be considered, respectively. Like the largest UDP-GlcNAc batch, UDP-GalNAc synthesis was done in 200 mL at 100 mM GalNAc concentration (Fig. 8).

Full conversion was reached after 29 h, equivalent to 12 g of UDP-GalNAc. TTN, STY, and average productivity were 20.34 $g_P*g_E^{-1}$, 2.07 $g*L^{-1}h^{-1}$, and 0.41 $g*h^{-1}$, respectively. Again, product formation is well described by the developed model. UDP-GalNAc was isolated by isopropanol precipitation at 32.1% purity with a 6.39 g (52.5%) yield. UDP-GalNAc isolation was confirmed by HPLC ESI-MS (**SI,** Figure S32).

4. Discussion

4.1. Simplifying enzyme availability, storage, and dosing

Three distinctive key factors for efficient UDP-GlcNAc and UDP-GalNAc synthesis were identified. The first was enzyme lyophilization as a major step towards scalability by separating expression and

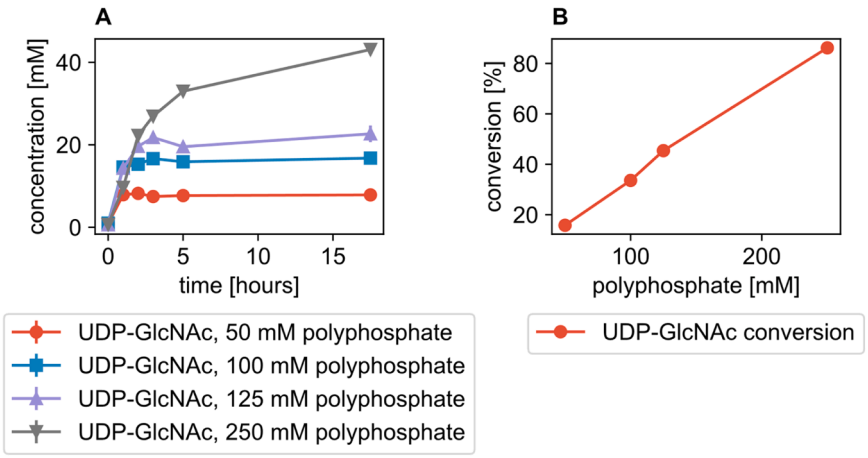

Fig. 6. UDP-GlcNAc synthesis with different polyphosphate-$MgCl_2$ combinations. Reaction conditions: *Ch*PPK: 0.66 mg (9.95 U), *Ec*CMPK: 0.33 mg (0.92 U), *Sc*CDPK: 0.33 mg (34.18 U), *Bl*NahK: 0.66 mg (0.86 U), *Hs*AGX1: 0.66 mg (3.83 U), *Pm*PpA: 0.66 mg, 50–250 mM polyphosphate, 20–100 mM $MgCl_2$, 2 mM AMP, 50 mM UMP, 50 mM GlcNAc, 200 mM HEPES-NaOH pH 8 in 1 mL, reaction time 17.5 h at 37 °C. A UDP-GlcNAc formation over reaction time for different polyphosphate-$MgCl_2$ combinations. B Influence of polyphosphate concentration on conversion percentage. Samples were measured in technical triplicates and standard deviations are shown as error bars (SI, Table S12–15).

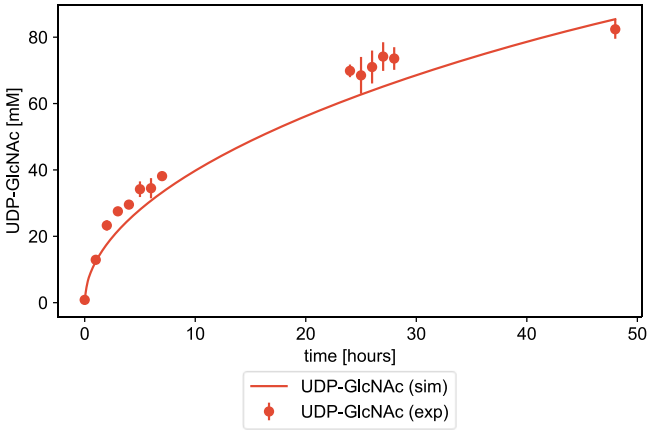

Fig. 7. UDP-GlcNAc synthesis in 200 mL volume. Reaction conditions: *Ch*PPK: 100 mg (1508 U), *Ec*CMPK: 90 mg (250 U), *Sc*CDPK: 40 mg (4144 U), *Bl*NahK: 150 mg (195 U), *Hs*AGX1: 140 mg (812 U), *Pm*PpA: 70 mg, 500 mM polyphosphate, 200 mM $MgCl_2$, 4 mM AMP, 100 mM UMP, 100 mM GlcNAc, 400 mM HEPES-NaOH pH 8 in 200 mL, reaction time 48 h at 37 °C. Samples were measured in technical triplicates and standard deviations are shown as error bars (SI, Table S16).

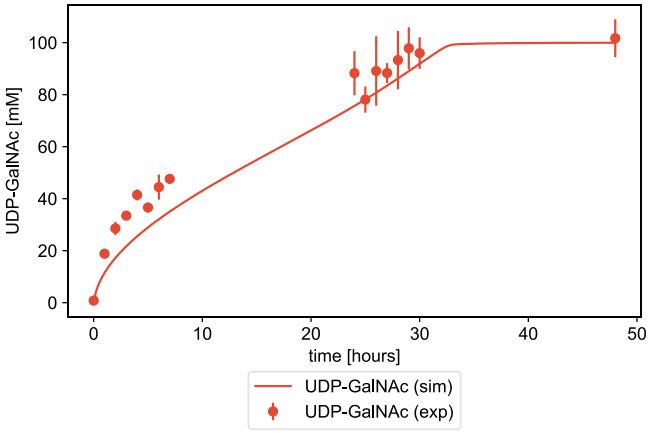

Fig. 8. UDP-GalNAc synthesis in 200 mL volume. Reaction conditions: *Ch*PPK: 100 mg (1508 U), *Ec*CMPK: 90 mg (250 U), *Sc*CDPK: 40 mg (4144 U), *Bl*NahK: 150 mg (195 U), *Hs*AGX1: 140 mg (812 U), *Pm*PpA: 70 mg, 500 mM polyphosphate, 200 mM $MgCl_2$, 4 mM AMP, 100 mM UMP, 100 mM GlcNAc, 400 mM HEPES-NaOH, pH 8 in 200 mL, reaction time 48 h at 37 °C. Samples were measured in technical triplicates and standard deviations are shown as error bars (SI, Table S17).

purification from their application in synthesis processes through improving shelf life. In addition, the dosing of the enzyme quantities and general handling are simplified, and storage is improved. We could retain 78–95% enzyme activity with a cascade half-life of 20 weeks (**SI,** Table S1**,** Figure S10).

4.2. *Finetuning and predicting cascade performance by modelling*

Second was the complex interplay of enzyme affinities and inhibitions. The long-established salvage pathway cascade for UDP-GlcNAc and UDP-GalNAc, consisting of *Bl*NahK, *Hs*AGX1, and *Pm*PpA (Fig. 1**A**), exhibits conversion-limiting inhibition by high ATP concentrations for *Bl*NahK and high ADP concentrations for *Hs*AGX1 [12]. Mitigating this by ATP regeneration [10,13,14], keeping ADP and ATP concentrations low, is prevented by the promiscuity of *Bl*NahK for UTP [25] (Fig. 2**B**), which is then, in turn, unavailable for product formation by *Hs*AGX1. This was not observed so far, as prior ATP regeneration systems used a class I *Ruegeria pomeroyi* PPK2 that converts occurring UDP back to UTP [10,13–15]. Therefore, *Ec*CMPK and *Sc*CDPK were introduced to generate UTP from UMP using ATP. Firstly, this enables the fine-tuning of ATP and UTP without relying on the set affinities of just one PPK enzyme, thereby mitigating the competition between ATP and UTP formation and slowing the activity of either BlNahK or HsAGX1. Secondly, it enables the process to start with AMP and UMP, which are significantly more affordable than ADP and UDP. In order to achieve the same result using a class I PPK, such as *Ruegeria pomeroyi* PPK3, two additional kinases would need to be considered. This would negate the advantage of using fewer different enzymes. With the cascade now consisting of six enzymes, considerable fine-tuning is necessary to prevent bottlenecks in product formation by enabling sufficient substrate access for each and avoiding inhibitor accumulation. Predictive kinetic modelling based on experimental data under process conditions is an excellent methodology to achieve this. We were able to obtain sufficient kinetic data for all enzymes (Table 1) to formulate rate equations for each involved substrate and product (**SI,** Table S2), well describing measured data and predicting cascade behavior in scaled-up

substrate concentrations from 10 to 100 mM and reaction volumes from 300 µL to 200 mL (Fig. 4, Fig. 7, Fig. 8, **SI,** Figure S29, Figure S30). Simplifications were made to the model regarding the reversible reaction of *Ch*PPK and enzyme inactivation, as these would add unnecessary complexity. The high ATP consumption and the resulting shift in equilibrium make a significant contribution of the reverse reaction highly unlikely. Additionally, all cascade enzymes exhibited high stability. Therefore, model prediction deviation from experimental measurements is most likely due to uncertainties in the kinetic modelling of enzyme parameters.

4.3. Considering the solubility of different magnesium phosphate species

Third was the interaction of different phosphate species with the necessary cofactor, magnesium, needed for all enzymes to retain activity. Polyphosphate has to be supplied at high molarities, as product formation is directly linked to it through ATP, which must be regenerated three times per product molecule. However, the consensus is that polyphosphate is used sequentially to phosphorylate nucleotides [18]. Therefore, even small polyphosphate molarities should be sufficient to supply the cascade with nucleotides, which is not the case for *Ch*PPK here, seemingly using only a fraction of the polyphosphate for phosphorylation. This has already been observed for different polyphosphate kinases showing varying polyphosphate usage efficiencies [26]. Additionally, for each product molecule, two orthophosphates are released by *Hs*AGX1 and *Pm*PpA. Magnesium phosphate solubility in water is well-researched and very low [27]. While data on exact magnesium polyphosphate solubility is scarce, the consensus is that the solubility in water is low, as it is commonly used as a sequestration agent [28,29]. We discovered that magnesium polyphosphate accessibility for the cascade is best at polyphosphate concentrations that were 2.5 times higher than $MgCl_2$ concentrations (Fig. 5). Magnesium polyphosphate preferences of the PPK from *Cytophaga* hutchinsonii are in stark contrast to the preferences of *Ruegeria pomeroyi* PPK from earlier works, which preferred a magnesium excess instead of a polyphosphate excess, with the best cascade performance at 32 mM polyphosphate and 120 mM $MgCl_2$ [10, 13]. However, the tested boundaries for *Ruegeria pomeroyi* PPK were already biased for magnesium excess with 20–40 mM polyphosphate and 80–120 mM $MgCl_2$, and polyphosphate excess was not screened further [10]. Still, for magnesium polyphosphate concentrations featuring a similar factor of a fourth between magnesium and polyphosphate concentration, cascade activity was very low here. As PPK activity is dependent on magnesium, polyphosphate, and nucleotide concentration in solution, differences in reaction media regarding a different choice of buffer and buffer concentration, as well as the uridine, could have an influence [10]. Additionally, *Cytophaga hutchinsonii* PPK proved to be dependent on higher polyphosphate concentrations in general (Fig. 6), so the choice of PPK most likely dictates the necessary magnesium polyphosphate concentrations. Additionally, different PPKs might prefer different forms of magnesium polyphosphate. While low magnesium concentrations lead to a coacervate formation, which is not cross-linked [30], facilitating PPK access to its surface, magnesium excess leads to cross-linking resembling polyphosphate granules with which some PPKs associate and others do not [31]. Still, both leave enough soluble magnesium to enable activity for magnesium cofactor dependent cascade enzymes. Loss of the magnesium cofactor for *Ec*CMPK, *Sc*CDPK, *Bl*NahK, and *Hs*AGX1 by phosphate precipitation was covered by introducing inhibition coefficients by reverse fitting experimental data to the developed model (Table 1). These coefficients were able to predict loss of activity over all ranges of phosphate concentrations and reaction volumes (Fig. 4, Fig. 7, Fig. 8, **SI,** Figure S29, Figure S30).

4.4. UDP-GlcNAc and UDP-GalNAc synthesis

We scaled both the UDP-GlcNAc and UDP-GalNAc synthesis to 100 mM substrate concentration and 200 mL volume. First, a repetitive batch approach was assessed (**SI,** Figure S30). Enzyme recovery by filtration was possible as described in earlier works [5], although flow through the membrane was impeded by precipitates. However, in comparison, against expectancy, activity could only be retained to a low extent regarding the first batch, contrary to earlier works [5]. That can probably be attributed to the unknown remaining magnesium, as well as polyphosphate and phosphate concentration that is partly carried into the new batch together with enzymes. With the addition of new magnesium and polyphosphate, the overall concentration of both can easily shift in a range unfavorable to cascade activity as described earlier (Fig. 5). Therefore, synthesis was conducted as a batch process. 10 g with 82.4% conversion (Fig. 7) and 12 g with full conversion were achieved (Fig. 8), respectively. UDP-GlcNAc was assessed with TTN, STY, and productivity determined at 16.95 $g_P{*}g_E^{-1}$, 1.04 $g{*}L^{-1}h^{-1}$, and 0.21 $g{*}h^{-1}$, respectively. Prior batch syntheses for UDP-GlcNAc including only NahK and GlmU showed STYs of 5.95 $g{*}L^{-1}h^{-1}$ and 4.25 $g{*}L^{-1}h^{-1}$, with the first one having a TTN of 7.15 $g_P{*}g_E^{-1}$ and the second one not providing a TTN [4]. Including ATP regeneration by *Rp*PPK−3 resulted in 2.85 $g{*}L^{-1}h^{-1}$ [13]. Fischöder showed a STY of 0.34 $g{*}L^{-1}h^{-1}$ and a high TTN of 522 $g_P{*}g_E^{-1}$ in a repetitive batch achieved by reusing the enzymes multiple times [5]. The discrepancy of the STY values reflects the increasing complexity of the enzyme cascades, their re-use, and possible side effects as demonstrated in the present work. Regarding enzyme efficiency, the TTN and STY refer to three more cascade enzymes in comparison. This also puts the lower productivity in a different light, which is quite acceptable when considering the more efficient use of enzymes and the scale-up. UDP-GalNAc was assessed with TTN, STY, and productivity determined at 20.34 $g_P{*}g_E^{-1}$, 2.07 $g{*}L^{-1}h^{-1}$, and 0.41 $g{*}h^{-1}$, respectively. Fischöder presented a STY of 0.24 $g{*}L^{-1}h^{-1}$ and a TTN of 398 $g_P{*}g_E^{-1}$ in a repetitive batch [5]. A similarly optimized batch for 50 mM substrate concentration showed a STY of 1.17 $g{*}L^{-1}h^{-1}$ compared to 2.07 $g{*}L^{-1}h^{-1}$ here, which indicates that STYs in this order of magnitude are the optimum achievable for high substrate batch process [10]. STYs compared to the processes without systematic kinetic optimization were significantly higher, while the lower TTNs are to be attributed to reusing the enzymes over multiple batches. Compared to UDP-GlcNAc, the UDP-GalNAc batch exhibited a higher rate of product formation. This can be attributed to three key differences in the enzyme kinetics (Table 1). First is the significantly higher v_{max} of 14.9 $U{*}mg^{-1}$ in case of UDP-GalNAc compared to only 5.8 $U{*}mg^{-1}$ in case of UDP-GlcNAc of *Hs*AGX1. Second is the difference in the side reaction of *Bl*NahK, sugar phosphorylation by UTP. In case of UDP-GlcNAc, this reaction considerably lowers the available UTP pool with a v_{max} of 0.68 $U{*}mg^{-1}$ compared to 1.3 $U{*}mg^{-1}$ for the reaction with ATP. For the UDP-GalNAc cascade, the *Bl*NahK reaction with UTP is substrate-inhibited by GalNAc with a K_I of 0.14 mM. Due to high GalNAc concentrations, this side reaction has no considerable negative influence on the available UTP pool. Third is the competition between *Bl*NahK and *Ec*CMPK for ATP. For UDP-GlcNAc, the affinities of both enzymes for ATP are similar at 0.1 mM, leading to strong competition. For UDP-GalNAc, the affinity of *Bl*NahK for ATP is 1.96 mM, making the *Ec*CMPK reaction the preferred one. All in all, these differences lead to a lower UTP availability in the UDP-GlcNAc cascade, which slows product formation compared to UDP-GalNAc, where UTP availability can be well maintained.

4.5. Product isolation by precipitation

Among the applied methods for nucleotide sugar purification [8] we choose precipitation of UDP-GlcNAc and UDP-GalNAc by isopropanol as previously applied for the isolation of GDP-fucose [11]. Product isolation for UDP-GlcNAc yielded 2.37 g (23.7%) with 24.6% purity, and for UDP-GalNAc 6.39 g (52.5%) with 32.1% purity. Contaminants were HEPES-NaOH, discovered in HPLC ESI-MS (**SI,** Figure S31—**32**), and likely different magnesium phosphate species prone to precipitation.

However, the yields and purity are low, which are attributed to the high content of polyphosphate in the starting product solutions. Further precipitation steps for polyphosphate and nucleosides by the addition of ethanol could be included prior to nucleotide sugar precipitation [32] Anion exchange chromatography (AEC) follows as next step to bind the nucleotide sugars. However, this process step requires high dilutions to bind the products, which in turn requires high column volumes and an extended process time. Moreover, elution of the nucleotide sugar with salts of monovalent cations (e.g. NaCl) is followed by a further precipitation step with ethanol to remove excess of the salt. Overall, the outlined alternative strategy includes several more steps, which may improve product purity but diminish product yields.

5. Conclusions

We scaled up a UDP-GlcNAc batch from 10 mM to 100 mM in 200 mL, achieving 10 g of product with a decent STY of 1.04 $g*L^{-1}h^{-1}$, a productivity of 0.21 $g*h^{-1}$, and an efficient TTN of 16.95 $g_P*g_E^{-1}$. We observed product formation limiting competition of *Bl*NahK and *Hs*AGX1 for UTP at low ATP concentrations. This was mitigated by introducing a fine-tuned, uncoupled UTP generation and ATP generation/regeneration system consisting of polyphosphate kinase *Ch*PPK and cytidine/uridine monophosphate kinase *Ec*CMPK, as well as cytidine/uridine diphosphate kinase *Sc*CDPK. Kinetic modelling of the cascade enabled us to minimize enzyme amounts, prevent intermediate accumulation, and balance especially the regeneration cassette according to substrate affinities. In order to achieve efficient product formation, we found that a sufficient supply of ATP is a crucial aspect for distribution amongst kinases, having dissimilar substrate affinities, for an equal supply of GlcNAc-1-P and UTP to *Hs*AGX1. We engaged the solubility challenge of magnesium phosphate species by studying the magnesium polyphosphate dependency of *Cytophaga hutchinsonii* PPK and discovered a ratio of polyphosphate to magnesium of 2.5 to work best, all while keeping the polyphosphate threshold high enough. All in all, we provide a methodology for efficient multi-gram production of UDP-GlcNAc with high yields. Additionally, the cascade with slight modifications can be used for UDP-GalNAc production as well, achieving full conversion of 12 g product in 200 mL with a STY of 2.07 $g*L^{-1}h^{-1}$, a productivity of 0.41 $g*h^{-1}$, and a TTN of 20.34 $g_P*g_E^{-1}$, and the established regeneration cassette is transferable to other nucleotide sugar-producing enzyme cascades. A precipitation protocol yielded 24% and 52% product recovery for UDP-GlcNAc and UDP-GalNAc, respectively. However, with the high content of polyphosphate, phosphate, and buffer salt in the product, this needs to be revisited to improve the feasibility of scaled-up production. Especially efficient phosphate and polyphosphate removal remains a challenge for product isolation with high purity and yield. Achieving this is a promising prospect for further research on nucleotide sugar cascades including polyphosphate and PPK nucleotide regeneration systems.

CRediT authorship contribution statement

Benjamin Schmitz: Writing – review & editing, Writing – original draft, Visualization, Methodology, Investigation, Formal analysis, Conceptualization. **Shubhang Sharma:** Writing – review & editing, Formal analysis. **Daniel Ohde:** Writing – review & editing, Supervision, Project administration, Formal analysis. **Andreas Liese:** Writing – review & editing, Supervision, Project administration, Funding acquisition. **Lothar Elling:** Writing – review & editing, Supervision, Resources, Project administration, Funding acquisition, Conceptualization.

Funding

This research was funded by financial support by the Federal Ministry of Research, Technology and Space (BMFTR) through the project BL1–8: BioProNuk (FKZ: 031B1146B) within the competence center Bio4MatPro: "Competence Center for the Biological Transformation of Materials Science and Production Engineering".

Declaration of Competing Interest

The authors declare that they have no known competing financial interests or personal relationships that could have appeared to influence the work reported in this paper.

Acknowledgment

The authors thank Oliver Wersin and Shunhang Hou for their support in conducting experiments.

Appendix A. Supporting information

Supplementary data associated with this article can be found in the online version at doi:10.1016/j.nbt.2026.06.008.

Data availability

Data will be made available on request.

References

[1] Salih ARC, Farooqi HMU, Amin H, Karn PR, Meghani N, Nagendran S. Hyaluronic acid: comprehensive review of a multifunctional biopolymer. Future J Pharm Sci 2024;10. https://doi.org/10.1186/s43094-024-00636-y.
[2] Ye H, Zhang R, Zhang C, Xia Y, Jin L. Advances in hyaluronic acid: bioactivity, complexed biomaterials and biological application: a review. Asian J Surg 2024. https://doi.org/10.1016/j.asjsur.2024.08.100.
[3] Gottschalk J, Assmann M, Kuballa J, Elling L. Repetitive synthesis of high-molecular-weight hyaluronic acid with immobilized enzyme cascades. ChemSusChem 2022;15:e202101071. https://doi.org/10.1002/cssc.202101071.
[4] Eisele A, Zaun H, Kuballa J, Elling L. In vitro one-pot enzymatic synthesis of hyaluronic acid from sucrose and N-acetylglucosamine: optimization of the enzyme module system and nucleotide sugar regeneration. ChemCatChem 2018;10: 2969–81. https://doi.org/10.1002/cctc.201800370.
[5] Fischöder T, Wahl C, Zerhusen C, Elling L. Repetitive batch mode facilitates enzymatic synthesis of the nucleotide sugars UDP-Gal, UDP-GlcNAc, and UDP-GalNAc on a multi-gram scale. Biotechnol J 2019;14. https://doi.org/10.1002/biot.201800386.
[6] Li S, Wang S, Wang Y, Qu J, Liu X-w, Wang PG, et al. Gram-scale production of sugar nucleotides and their derivatives. Green Chem 2021;23:2628–33. https://doi.org/10.1039/d1gc00711d.
[7] Volpi N. Therapeutic applications of glycosaminoglycans. Curr Med Chem 2006;13: 1799–810. https://doi.org/10.2174/092986706777452470.
[8] Frohnmeyer H, Elling L. Enzyme cascades for the synthesis of nucleotide sugars: updates to recent production strategies. Carbohydr Res 2023;523:108727. https://doi.org/10.1016/j.carres.2022.108727.
[9] Frohnmeyer H, Kodra N, Elling L. Advanced enzymatic multigram-scale production of nucleotide sugars in a continuous fed-batch membrane reactor. J Biotechnol 2024;395:1–11. https://doi.org/10.1016/j.jbiotec.2024.09.001.
[10] Hoang TS, Wormstall ST, Hoang NH, Reichl U, Rexer TFT. Establishment of a cell-free multi-enzyme cascade for the synthesis of UDP-GalNAc. N Biotechnol 2025;89: 20–8. https://doi.org/10.1016/j.nbt.2025.05.003.
[11] Frohnmeyer H, Rueben S, Elling L. Gram-scale production of GDP-β-l-fucose with multi-enzyme cascades in a repetitive-batch mode. ChemCatChem 2022;14. https://doi.org/10.1002/cctc.202200443.
[12] Frohnmeyer H, Verkade JMM, Spiertz M, Rentsch A, Hoffmann N, Sobota M, et al. Process development for the enzymatic gram-scale production of the unnatural nucleotide sugar UDP-6-Azido-GalNAc. ChemSusChem 2024;17:e202400311. https://doi.org/10.1002/cssc.202400311.
[13] Gottschalk J, Blaschke L, Aßmann M, Kuballa J, Elling L. Integration of a nucleoside triphosphate regeneration system in the one-pot synthesis of UDP-sugars and hyaluronic acid. ChemCatChem 2021;13:3074–83. https://doi.org/10.1002/cctc.202100462.
[14] Mahour R, Klapproth J, Rexer TFT, Schildbach A, Klamt S, Pietzsch M, et al. Establishment of a five-enzyme cell-free cascade for the synthesis of uridine diphosphate N-acetylglucosamine. J Biotechnol 2018;283:120–9. https://doi.org/10.1016/j.jbiotec.2018.07.027.
[15] Mahour R, Lee JW, Grimpe P, Boecker S, Grote V, Klamt S, et al. Cell-free multi-enzyme synthesis and purification of uridine diphosphate galactose. Chembiochem 2022;23:e202100361. https://doi.org/10.1002/cbic.202100361.
[16] Motomura K, Hirota R, Okada M, Ikeda T, Ishida T, Kuroda A. A new subfamily of polyphosphate kinase 2 (class III PPK2) catalyzes both nucleoside monophosphate phosphorylation and nucleoside diphosphate phosphorylation. Appl Environ Microbiol 2014;80:2602–8. https://doi.org/10.1128/AEM.03971-13.

[17] Nocek BP, Khusnutdinova AN, Ruszkowski M, Flick R, Burda M, Batyrova K, et al. Structural insights into substrate selectivity and activity of bacterial polyphosphate kinases. ACS Catal 2018;8:10746–60. https://doi.org/10.1021/acscatal.8b03151.
[18] Neville N, Roberge N, Jia Z. Polyphosphate kinase 2 (PPK2) enzymes: structure, function, and roles in bacterial physiology and virulence. Int J Mol Sci 2022;23. https://doi.org/10.3390/ijms23020670.
[19] Wahl C, Hirtz D, Elling L. Multiplexed capillary electrophoresis as analytical tool for fast optimization of multi-enzyme cascade reactions - synthesis of nucleotide sugars: dedicated to Prof. Dr. Vladimir Kren on the occasion of his 60(th) birthday. Biotechnol J 2016;11:1298–308. https://doi.org/10.1002/biot.201600265.
[20] Peneff C, Ferrari P, Charrier V, Taburet Y, Monnier C, Zamboni V, et al. Crystal structures of two human pyrophosphorylase isoforms in complexes with UDPGlc (Gal)NAc: role of the alternatively spliced insert in the enzyme oligomeric assembly and active site architecture. EMBO J 2001;20:6191–202. https://doi.org/10.1093/emboj/20.22.6191.
[21] Sato M, Arakawa T, Nam YW, Nishimoto M, Kitaoka M, Fushinobu S. Open-close structural change upon ligand binding and two magnesium ions required for the catalysis of N-acetylhexosamine 1-kinase. Biochim Biophys Acta 2015;1854:333–40. https://doi.org/10.1016/j.bbapap.2015.01.011.
[22] R. Frostig, M. Johnson, C. Leary, Compiling machine learning programs via high-level tracing, 2018.
[23] R C, Harris, Millman KJ, van der Walt SJ, R, Gommers, et al. Array programming with NumPy. Nature 2020;585:357–62. https://doi.org/10.1038/s41586-020-2649-2.
[24] Virtanen P, Gommers R, Oliphant TE, Haberland M, Reddy T, Cournapeau D, et al. SciPy 1.0: fundamental algorithms for scientific computing in Python. Nat Methods 2020;17:261–72. https://doi.org/10.1038/s41592-019-0686-2.
[25] Koszagova R, Palencarova K, Nahalka J. Active inclusion bodies in the multienzymatic synthesis of UDP-N-acetylglucosamine. Int J Mol Sci 2025;26. https://doi.org/10.3390/ijms26199679.
[26] Achbergerova L, Nahalka J. Polyphosphate–an ancient energy source and active metabolic regulator. Microb Cell Fact 2011;10:63. https://doi.org/10.1186/1475-2859-10-63.
[27] Taylor AW, Frazier AW, Gurney EL, Smith JP. Solubility products of di- and trimagnesium phosphates and the dissociation of magnesium phosphate solutions. Trans Faraday Soc 1963;59. https://doi.org/10.1039/tf9635901585.
[28] Irani RD, Callis CF. Calcium and magnesium sequestration by sodium and potassium polyphosphates. J Am Oil Chem' Soc 2018;39:156–9. https://doi.org/10.1007/bf02632750.
[29] Onaka T, Miyajima T, Ohashi S. On the binding of magnesium to long-chain polyphosphate ions. J Inorg Nucl Chem 1981;43:3323–7. https://doi.org/10.1016/0022-1902(81)80110-8.
[30] Pfanstiel R, Iler RK. Magnesium polymetaphosphate. J Am Chem Soc 2002;78:5510–1. https://doi.org/10.1021/ja01602a014.
[31] Rosigkeit H, Kneissle L, Obruca S, Jendrossek D. The multiple roles of polyphosphate in Ralstonia eutropha and other bacteria. Microb Physiol 2021;31:163–77. https://doi.org/10.1159/000515741.
[32] Kulmer ST, Gutmann A, Lemmerer M, Nidetzky B. Biocatalytic cascade of polyphosphate kinase and sucrose synthase for synthesis of nucleotide-activated derivatives of glucose. Adv Synth Catal 2017;359:292–301. https://doi.org/10.1002/adsc.201601078.